Intermediate-spin states of ^{92}Zr and a large $B(E2)$ value between the 10_1^+ and 8_1^+ states

M. Sugawara*
Chiba Institute of Technology, Narashino, Chiba 275-0023, Japan

Y. Toh, M. Koizumi, M. Oshima, A. Kimura, T. Kin, and Y. Hatsukawa
Japan Atomic Energy Agency, Tokai, Ibaraki 319-1195, Japan

H. Kusakari
Chiba University, Inage-ku, Chiba 263-8522, Japan

(Received 3 June 2017; revised manuscript received 29 June 2017; published 21 August 2017)

This study investigated intermediate-spin states of ^{92}Zr via the inverse reaction ^{9}Be(^{86}Kr,3n)^{92}Zr. Seven transitions were newly observed, and a lifetime was extracted for the 10_1^+ state by analysis of Doppler-broadened line shapes of decay γ rays. A large $B(E2)$ value was obtained for the transition from 10_1^+ to 8_1^+, and the magnitude was comparable to that for the deformed excited configurations in ^{94}Zr that have recently been established. A possible origin for such collectivity is discussed qualitatively based on a phenomenological deformed rotor model. Moreover, a multipletlike structure that fits into the systematics for $N = 52$ even-A isotones is revealed for the negative-parity yrast states.

DOI: 10.1103/PhysRevC.96.024314

I. INTRODUCTION

Understanding how coexisting structures change along an isotopic chain or an isotonic chain is one of the most interesting questions in the study of nuclear structures [1]. In this respect, zirconium isotopes offer a quite challenging field of study. Roughly speaking, they show a rapid shape transition from spherical ground states for $A = 90$–98 to deformed ground states for $A = 100$ and heavier. However, if we look closely at the systematics of the 2_1^+ excitation energy, we recognize a sudden increase then decrease in excitation energy, reflecting the subshell closure at $N = 56$, on the way to the deformed region [2].

Coexisting structures were first suggested to exist around ^{100}Zr [3], and evidence of these structures has gradually extended to the lighter region. We now have evidence for coexisting structures in ^{94}Zr [4] and ^{96}Zr [5]. A $B(E2; 2_2^+ \rightarrow 0_2^+)$ as large as 18 W.u. has been deduced in ^{94}Zr based on results from the β^- decay of ^{94}Y and inelastic neutron scattering. The corresponding $B(E2)$ value of 36 W.u. in ^{96}Zr has been obtained by high-resolution inelastic electron scattering.

^{92}Zr is just next to the lighter edge of the shape-coexistence region that has been established to date. Although the excitation energies of 0_2^+ and 2_2^+ in ^{92}Zr are known to be 1.383 and 1.847 MeV, respectively [6], the $B(E2)$ values between these states have not yet been measured. Here, it is worth noting that the excitation energies of 0_2^+ and 2_2^+ in ^{92}Zr are very similar to those in ^{94}Zr (1.3 and 1.671 MeV, respectively, in ^{94}Zr). If these excitation energies are extrapolated to the intermediate-spin region based on a simple rotational relation, we can see them intruding into the near-yrast region. Therefore, it might be possible to recognize the influential role of the deformed configurations in either ^{92}Zr or ^{94}Zr by studying the electromagnetic properties of intermediate-spin states. Pantelica *et al.* [7] investigated high-spin states in ^{94}Zr through fission following heavy-ion fusion reactions. Unfortunately information on the electromagnetic properties of the intermediate-spin states was not obtained in that experiment.

These peculiar structures of Zr isotopes have attracted much attention from a theoretical perspective, and a number of large-scale conventional shell-model calculations have been performed [2,8]. These calculations reproduced the experimental data up to $N = 58$ rather accurately but were not used above $N = 60$. Recently, a large-scale Monte Carlo shell-model calculation was carried out for even-even Zr isotopes of $N = 50$–70 with a fixed Hamiltonian. This successfully described both the abrupt shape change occurring in the ground state at $N = 60$ and the shape-coexistence phenomena associated with it [9].

High-spin states of ^{92}Zr were investigated previously by Brown *et al.* [10], Korschinek *et al.* [11], Fotiades *et al.* [12], Regan *et al.* [13], and Pantelica *et al.* [7]. Wang *et al.* recently extended the level scheme over the (14^+) state [14] up to $E_x \sim 11$ MeV. The lifetime of the 4_1^+ state was measured by Mach *et al.* [15] using a β-γ-γ fast timing method. The lifetime of the 8_1^+ state was first measured by Korschinek *et al.* [11] and was recently remeasured by Bucurescu *et al.* [16]. The lifetimes of excited low-spin states were extensively investigated by Fransen *et al.* through the $(n,n'\gamma)$ reaction [6].

The present paper reports an in-beam γ-ray study of intermediate-spin states of ^{92}Zr through the inverse reaction ^{9}Be(^{86}Kr,3n)^{92}Zr. Although we could not extend the previous level scheme to higher-spin states, seven transitions were newly identified in the intermediate-spin region, and these observations revealed a multipletlike structure of the negative-parity yrast states. Moreover, a lifetime was extracted for the 10_1^+ state by analysis of Doppler-broadened line shapes

*masahiko.sugawara@it-chiba.ac.jp

TABLE I. Properties of γ rays observed in this experiment. Relative intensities are normalized to the intensity of the 934-keV transition from 2^+ to 0^+. The ADO ratios are tabulated for different combinations of detectors.

$I_i \rightarrow I_f$	E_γ (keV)	I_γ	ADO (47°/90°)	ADO (147°/90°)	Multipolarity
$(14^+) \rightarrow (12^+)$	89.1(5)	0.12(1)			
$(9^-) \rightarrow (8^-)$	179.0(5)	4.3(3)	0.99(4)	0.83(4)	Dipole
$(10^-) \rightarrow (9^-)$	215.4(5)	1.2(1)	1.31(6)	1.22(6)	Mixed
$(14^+) \rightarrow (13^+)$	240.8(5)	0.22(2)	0.62(6)	0.51(7)	Dipole
$(15^+) \rightarrow (14^+)$	250.1(5)	0.096(8)	0.67(10)	0.77(16)	Dipole
$8^+ \rightarrow 6^+$	351.0(5)	34(3)	1.39(6)	1.47(6)	Quadrupole
$(11^-) \rightarrow (9^-)$	351.0(5)	0.71(10)	1.29(8)	1.95(12)	Quadrupole
$(10^-) \rightarrow (8^-)$	394.5(5)	0.14(2)	1.15(25)	1.22(33)	Quadrupole
$(15^+) \rightarrow (14^+)$	402.0(5)	0.04(2)	0.82(13)	0.74(15)	Dipole
$7^- \rightarrow 6^+$	421.6(5)	1.09(10)	0.83(6)	0.67(6)	Dipole
$(8^-) \rightarrow 7^-$	439.0(5)	8.5(7)	0.71(3)	0.64(3)	Dipole
$6^+ \rightarrow 5^-$	471.0(5)	1.9(2)	0.57(3)	0.44(3)	Dipole
$(18^+) \rightarrow (16^+)$	531.4(5)	0.13(2)	1.23(11)	0.98(11)	Quadrupole
$6^+ \rightarrow 4^+$	558.6(5)	1.44(12)			
$4^+ \rightarrow 2^+$	560.4(5)	95(8)	1.29(5)	1.36(5)	Quadrupole
$(9^-) \rightarrow 7^-$	618.4(5)	3.7(3)	1.41(9)	1.45(9)	Quadrupole
$(12^+) \rightarrow 10^+$	650.0(5)	10.3(8)	1.39(6)	1.56(7)	Quadrupole
$7^- \rightarrow 5^-$	893.4(5)	19(2)	1.44(6)	1.29(5)	Quadrupole
$4^+ \rightarrow 4^+$	902.4(5)	1.8(2)	0.84(5)	0.94(7)	Mixed
$2^+ \rightarrow 0^+$	934.1(5)	100(10)			
$10^+ \rightarrow 8^+$	987.5(5)	18.5(15)	1.34(6)	1.43(6)	Quadrupole
$5^- \rightarrow 4^+$	990.1(5)	32(3)	1.04(4)	0.90(4)	Dipole
$(17^+) \rightarrow (16^+)$	1005.8(5)	0.072(8)	0.70(24)	1.06(33)	Dipole
$(17^+) \rightarrow (15^+)$	1046.6(5)	0.17(2)			
$(14^+) \rightarrow (12^+)$	1098.0(5)	3.5(3)	1.53(8)	1.53(9)	Quadrupole
$(14^+) \rightarrow (14^+)$	1109.0(5)	0.25(2)	1.36(15)	1.47(19)	$\Delta I = 0$ dipole
$(15^+) \rightarrow (14^+)$	1359.4(5)	0.25(2)	0.54(6)	0.47(7)	Dipole
$(16^+) \rightarrow (14^+)$	1399.9(5)	0.84(7)	1.70(18)	1.98(23)	Quadrupole
$6^+ \rightarrow 4^+$	1461.6(5)	39(3)	1.25(5)	1.34(5)	Quadrupole
$(13^+) \rightarrow (12^+)$	1966.1(5)	0.21(2)	0.47(6)	0.39(7)	Dipole

of decay γ rays. A large $B(E2)$ value was obtained for the transition from 10_1^+ to 8_1^+ and, remarkably, its magnitude was comparable to that of the deformed excited configurations in ^{94}Zr. Experimental details and results are presented in Sec. II, the results are discussed in Sec. III, and a summary is given in Sec. IV.

II. EXPERIMENTAL METHODS AND RESULTS

The intermediate-spin states of ^{92}Zr were populated through the inverse reaction ^{9}Be(^{86}Kr,3n)^{92}Zr. A ^{9}Be foil with a thickness of 1.5 mg/cm^2 on a Au backing of 30 mg/cm^2 was bombarded with a 280-MeV ^{86}Kr beam provided by the tandem accelerator at the Japan Atomic Energy Agency (JAEA). The γ rays emitted from the excited states were detected with an array of 12 HPGe detectors with bismuth germanate Compton suppressors [17,18]. The HPGe detectors were placed at angles of 47°, 72°, 90°, 105°, and 147° with respect to the beam direction. The energy resolutions of the HPGe detectors were 2.3–4.4 keV at 1.4 MeV. The experimental data were recorded on magnetic tapes event by event for events with multiplicities of two or greater. A total of 2.2×10^8 events were collected during 3 days of beam time. The multiple γ-γ coincidence events were sorted into E_γ-E_γ matrices, and the level scheme was constructed from these matrices using the software developed by Radford [19]. The γ-ray efficiency curve was obtained from the measurements of ^{133}Ba and ^{152}Eu sources after the experiment and was input into the analysis software. The relative intensities of the γ rays were obtained from the gated spectra.

Spins of excited levels were assigned by using the γ-ray coincidence intensity ratios $I(\gamma_1$:47°,γ_2:all)/$I(\gamma_1$:90°,γ_2:all), and $I(\gamma_1$:147°,γ_2:all)/$I(\gamma_1$:90°,γ_2:all) angular distribution from oriented states [(ADO) ratios] [20]. Here, $I(\gamma_1$:θ,γ_2:all) corresponds to the γ-ray coincidence intensity observed by the detectors at angle θ by setting the gates on the detectors to allow any angle. We sorted γ-γ coincidence events into five asymmetric matrices whose x axes were the γ-ray energies in the detector at 47°, 72°, 90°, 105°, or 147° and whose y axes were the γ-ray energies in the detector at any position in common. These matrices were used subsequently to obtain ADO ratios. Typical ADO ratios observed for the known γ rays in the present experiment were 1.3 for stretched quadrupole transitions and 0.8 for stretched pure dipole transitions. Therefore, we assigned the stretched quadrupole transition (stretched dipole transition) to ratios around 1.3 (around 0.8) for the new γ rays. The properties of γ rays observed in the present experiment are summarized in Table I.

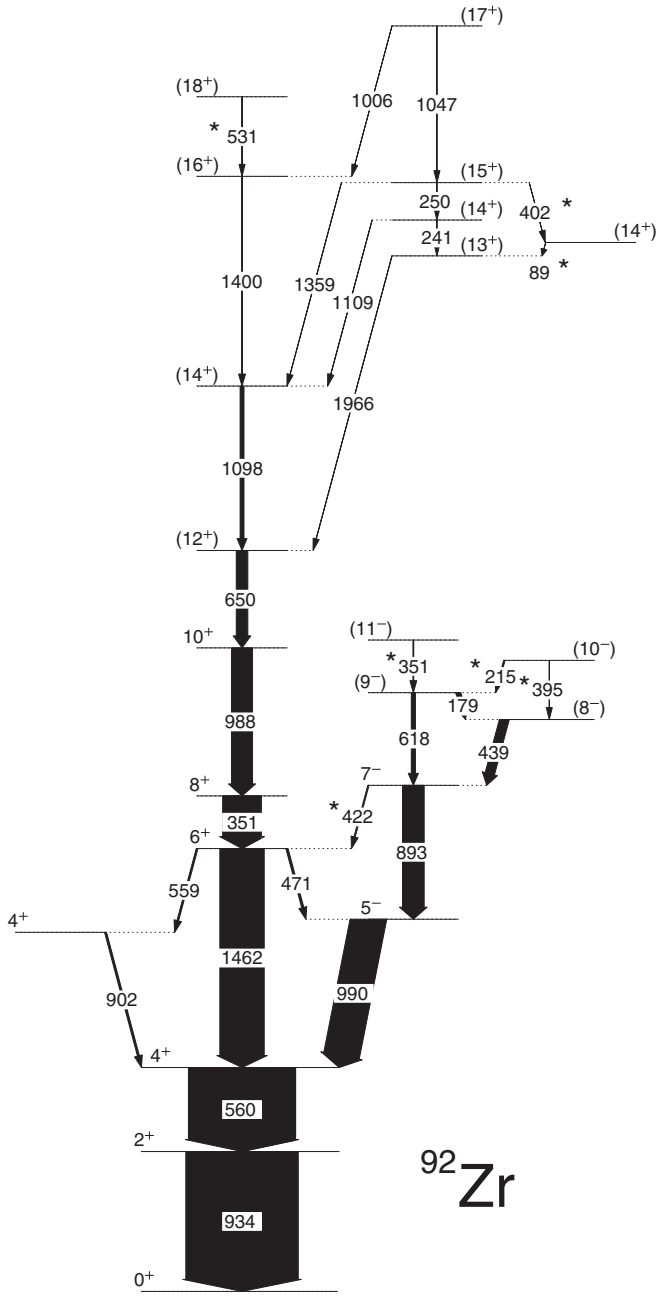

FIG. 1. Proposed level scheme of ^{92}Zr based on an analysis of the E_γ-E_γ matrix. Newly observed transitions are marked with asterisks.

The level scheme for ^{92}Zr established in this experiment is shown in Fig. 1. Examples of γ-γ coincidence spectra are given in Fig. 2. We confirmed the yrast positive-parity states up to (16^+) as observed by Wang *et al.* [14]. A new transition of 531 keV, which was not observed by Wang *et al.* [14], can be seen in the spectrum obtained by setting a gate on the 650-keV transition from (12^+) to 10^+. Because this transition probably has quadrupole character based on its ADO ratio in Table I, a new (18^+) state has been added above the (16^+) state.

Although we could not identify the levels above that, six transitions were newly added to the level scheme in the intermediate-spin region as described below.

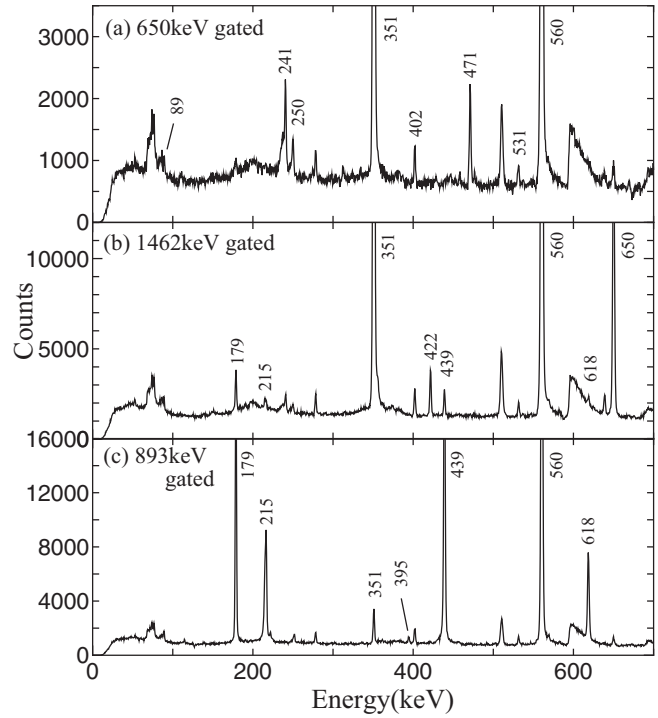

FIG. 2. Examples of γ-γ coincidence spectra. These spectra were obtained from the E_γ-E_γ matrix and provide evidence for the newly observed transitions. Energy values are given above the peaks in units of keV. (a) A spectrum obtained by setting a gate on the 650-keV transition from (12^+) to 10^+. (b) A spectrum obtained by setting a gate on the 1462-keV transition from 6^+ to 4^+. (c) A spectrum obtained by setting a gate on the 893-keV transition from 7^- to 5^-.

Two new γ rays of 89 and 402 keV can be seen in Fig. 1(a). These transitions coincide with each other, and their sum is equal to the sum of the 241- and 250-keV transitions between (13^+) and (15^+). Therefore, a new (14^+) state has been added, adopting this order from the γ-ray intensity relation. Moreover, a new transition of 422 keV can be seen in the spectrum obtained by setting a gate on the 1462-keV transition from 6^+ to 4^+ in Fig. 1(b). Since this energy precisely conforms to the difference between 893 and 471 keV, the new transition of 422 keV is placed between 7^- and 6^+. Furthermore three new transitions of 215, 351, and 395 keV can be seen in the spectrum obtained by setting a gate on the 893-keV transition from 7^- to 5^- in Fig. 1(c). Combining the information about coincidence relations, intensity relations, and ADO ratios has led us to propose a multipletlike structure that consists of the 7^-, (8^-), (9^-), (10^-), and (11^-) states. Summarizing, we have identified seven new transitions in total.

Because we used a target with a backing that was thick enough for residuals to stop inside it, the lifetimes of the high-spin states could be extracted from the Doppler-broadened line shapes of the decay γ rays. To obtain the angle-dependent γ-ray spectra, we used the five asymmetric matrices that were made for the ADO analysis. The five angle-dependent γ-ray spectra were obtained by setting a gate on each of the three lowest $E2$ cascades in the positive-parity states, that is, the

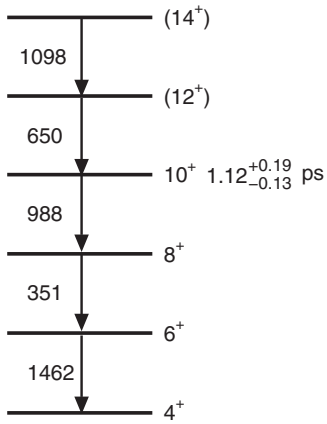

FIG. 3. Partial level scheme included in the lifetime analysis. Energies of γ transitions are given in keV. Deduced mean life is shown on the right of the 10^+ state with statistical uncertainties.

934-, 560-, and 1462-keV transitions. Various combinations of these spectra subsequently were used for the lifetime analysis.

The observed γ-ray line shapes in the five angle-dependent spectra were analyzed simultaneously with the code LINESHAPE developed by Wells and Johnson [21]. A Monte Carlo simulation was performed with a time step of 0.0011 ps for 10 000 histories to generate a velocity profile of residuals in the target and backing. The electronic stopping power was calculated according to the formula with the shell correction of Northcliffe and Schilling [22].

The energies of the γ transitions in the cascade of interest and the side-feeding intensities were used as the input parameters for the line-shape analysis. The side-feeding intensities were obtained from the gated spectra at 90° and fixed in the fitting procedure. The level structure is irregular in the energy region of interest, so the side feeding into each level in the cascade was assumed to be through a single level on the principle of being as simple as possible. For each line-shape combination, the in-cascade and side-feeding lifetime, the background parameters and intensities of contaminant peaks were allowed to vary. The χ^2 minimization routines of MINUIT [23] were used to fit the simulated line shapes to the observed spectra.

The levels of interest in the present paper are among the yrast states. Since the intensity of the 1400-keV transition is only a quarter of that of the 1098-keV transition, levels under the (14^+) state were included in the analysis as shown in Fig. 3. To begin, the highest transition of the cascade was assumed to be 100% fed effectively from a single upper level. The other parameters were allowed to vary until the minimum χ^2 value was reached. This was taken as the effective lifetime for the (14^+) level. This effective lifetime then was used as the input parameter to deduce the side-feeding lifetime to and the lifetime of the next lower level in the cascade. The χ^2 minimization process for each individual level was repeated in this way down to the lowest level of the cascade. Finally, the lifetimes of all the states in the cascade were deduced from a global fit of the full cascade in which only the in-cascade and side-feeding lifetimes were allowed to vary. The uncertainties

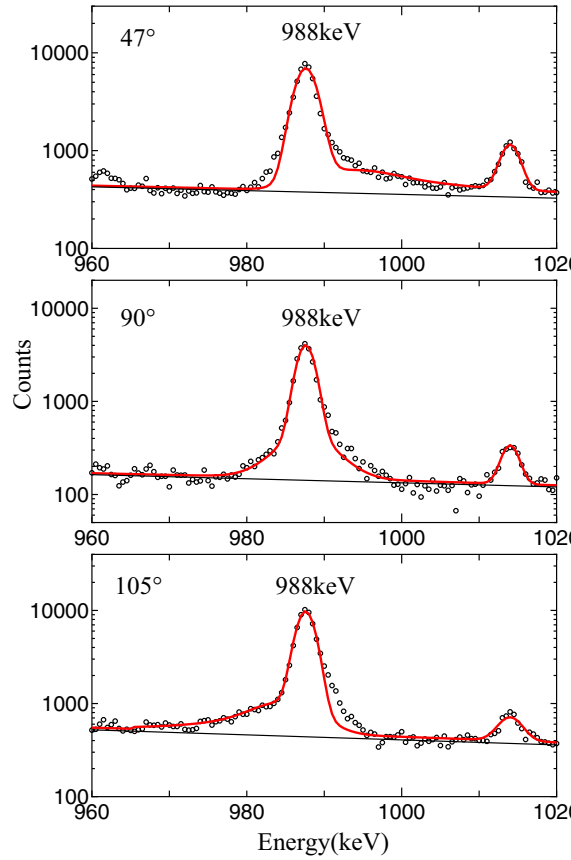

FIG. 4. Examples of the line-shape fits for the 988-keV transition at 47°, 90°, and 105° with respect to the beam direction. Results of the fits to the experimental spectra are shown as thick lines. A contaminant peak at 1014 keV is included.

in the lifetime measurements were obtained from the χ^2 behavior in the vicinity of the minimum for the simultaneous fit for the five angle-dependent spectra using the MINOS [23] routine. The other source of statistical error was the uncertainty in the side-feeding intensity, which was estimated to be 5%. The final statistical uncertainty was obtained by adding these two uncertainties in quadrature.

In the course of the analysis, it was found that only the transitions below the 10^+ state have an observable in-flight decay component. Therefore, we could extract a meaningful lifetime for only the 10^+ level as shown in Fig. 3 where the mean life and the statistical uncertainties are given. Here, it is worth noting that the feeding from the (16^+) state contributes only 5% of the 988-keV transition. Since there is a systematic uncertainty as large as 20% based on stopping powers, the measured mean life for the 10^+ state is $\tau = 1.12^{+0.19}_{-0.13}$ ps (statistical) ± 0.22 ps (systematic). Moreover, note that the side-feeding lifetime for the 10^+ level is of the same order of magnitude.

Examples of line-shape fits for the 988-keV transition in the cascade are shown in Fig. 4. The deduced $B(E2)$ values are given in Table II which clearly shows an unexpectedly large $B(E2)$ value for spherical nuclei. If we assume a simple rotational model and extrapolate down to the lower-spin states,

TABLE II. Deduced $B(E2)$ values in the present experiment. The corresponding statistical errors are given in parentheses. The $B(E2)$ values for the lower transitions in the yrast cascade also are shown for comparison.

$I_i^\pi \rightarrow I_f^\pi$	$B(E2)$ $(eb)^2$	$B(E2)$ W.u.	Reference
$10^+ \rightarrow 8^+$	$0.077(^{+13}_{-9})$	$31(^{+5}_{-4})$	
$8^+ \rightarrow 6^+$	0.0089(5)	3.6(2)	[11]
$8^+ \rightarrow 6^+$	0.0134(2)	5.4(1)	[16]
$4^+ \rightarrow 2^+$	0.0100(3)	4.1(1)	[15]
$4^+ \rightarrow 2^+$	0.0099(5)	4.0(2)	[16]
$2^+ \rightarrow 0^+$	0.0166(10)	6.7(4)	[15]

this $B(E2: 10^+ \rightarrow 8^+)$ of 31 W.u. corresponds to a $B(E2: 2^+ \rightarrow 0^+)$ of 18 W.u. that is the same magnitude as for the deformed configuration which has been measured in ^{94}Zr [4].

III. DISCUSSION

The remarkable results of the present paper are the observation of the unexpectedly large $B(E2)$ value for the transition from 10_1^+ to 8_1^+ and the identification of the multipletlike structure for the negative-parity yrast states. Therefore, the discussion below is focused on these points.

A. A possible origin of the unexpectedly large $B(E2)$ value

To begin, we reexamine the shape phase transition observed in Zr isotopes with neutron numbers between 50 and 60, including not only 2^+ states, but also higher-spin states. A good way to reveal such behavior is to plot excitation energy as a function of spin. Figure 5 shows the systematics of E_x vs I for the positive-parity yrast states up to 14^+ of even-even Zr isotopes ranging from $N = 50$ to $N = 60$. We clearly can see different behaviors in three different categories: (a) subshell closed structures, such as ^{90,96}Zr, (b) intermediate structures, such as ^{92,94,98}Zr, and (c) deformed structures, such as ^{100}Zr.

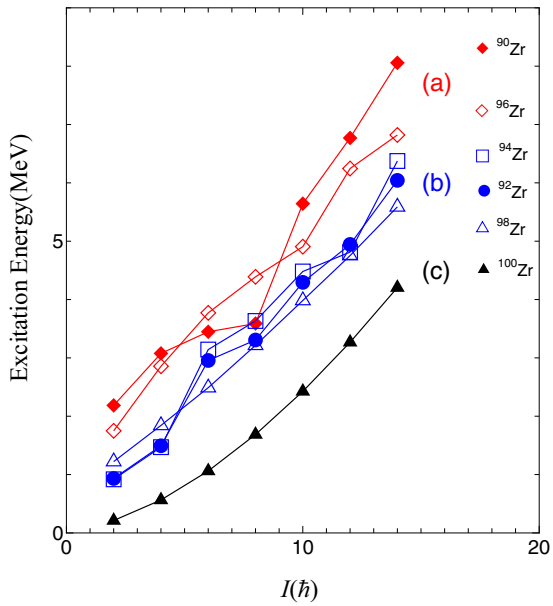

FIG. 5. Systematics of E_x vs I for the positive-parity yrast states up to 14^+ of even-even Zr isotopes ranging from $N = 50$ to $N = 60$. (a) The subshell closed structures ^{90,96}Zr, (b) the intermediate structures ^{92,94,98}Zr, and (c) the deformed structure ^{100}Zr.

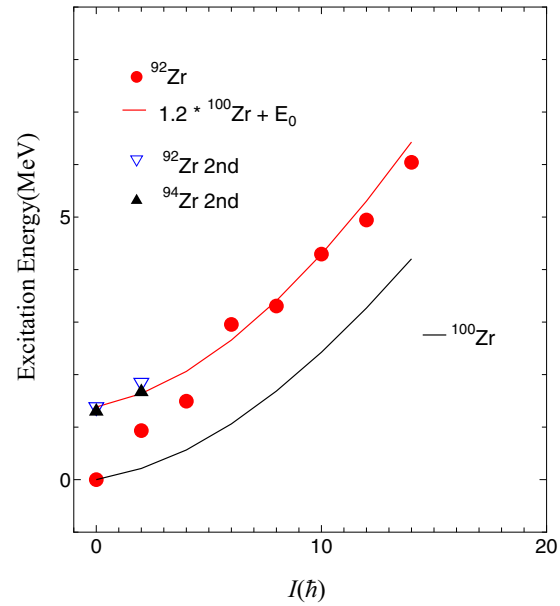

FIG. 6. Comparison of E_x vs I in ^{92}Zr from the experiment with a phenomenological curve for an excited deformed rotor. The phenomenological curve is for an excitation energy of $E_0 + 1.2 \times$ gsb (ground-state band) of ^{100}Zr. Here, E_0 stands for the excitation energy of the 0_2^+ state. The corresponding data points for the known 0_2^+ and 2_2^+ states in ^{92}Zr and ^{94}Zr also are included in the figure.

As mentioned in the Introduction, the excitation energies of 0_2^+ and 2_2^+ in ^{92}Zr are very similar to those in ^{94}Zr, between which a large $B(E2)$ value has been obtained experimentally. Moreover, the observed $B(E2: 10^+ \rightarrow 8^+)$ is comparable with the magnitude for the deformed configuration in ^{94}Zr if we assume a simple rotational model. Therefore, it is conceivable that a coexisting deformed structure as in ^{94}Zr might be a possible origin of the large $B(E2)$ value observed in this experiment. To examine that hypothesis qualitatively, the experimental plot of E_x vs I in ^{92}Zr is compared in Fig. 6 with a phenomenological curve for an excited deformed rotor with an energy of $E_0 + 1.2 \times$ gsb of ^{100}Zr. Here, E_0 stands for the excitation energy of the 0_2^+ state in ^{92}Zr. The corresponding data points for the known 0_2^+ and 2_2^+ states in ^{92}Zr and ^{94}Zr also are included in the figure for comparison.

B. On the multipletlike structure of the negative-parity yrast states

To see the general features of the negative-parity yrast states, the systematics plot of E_x vs I is shown in Fig. 7 for even-even Zr isotopes ranging from $N = 50$ to $N = 60$. Here, we again can see different behaviors in different categories as in the case of the positive-parity yrast states discussed in the previous subsection.

To generate negative-parity states in Zr isotopes, an odd number of proton excitations from $(2p_{3/2}, 1f_{5/2}, 2p_{1/2})$

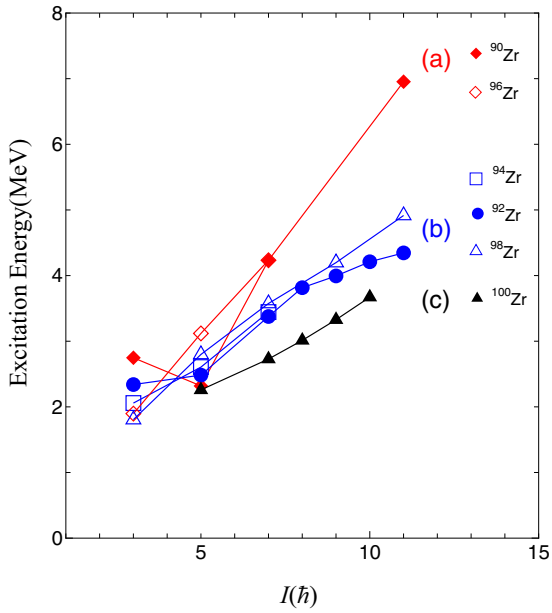

FIG. 7. Systematics of E_x vs I for the negative-parity yrast states up to 11^- of even-even Zr isotopes ranging from $N = 50$ to $N = 60$. (a) The subshell closed structures ^{90,96}Zr, (b) the intermediate structures ^{92,94,98}Zr, and (c) the deformed structure ^{100}Zr.

to $1g_{9/2}$ orbits is required. The lowest of such excitations is $\pi(2p_{1/2}^{-1}1g_{9/2})_{5^-}$ in even-A isotopes and $[\pi(2p_{1/2}^{-1}1g_{9/2})\nu 2d_{5/2}]_{15/2^-}$ in odd-A isotopes. Systematics for these excitations are shown in Fig. 8. Since the configurations for the 6^+ and 8^+ yrast states are expected to be $\pi(2p_{1/2}^{-2}1g_{9/2}^2)_{6,8^+}$, those also are included in the figure for

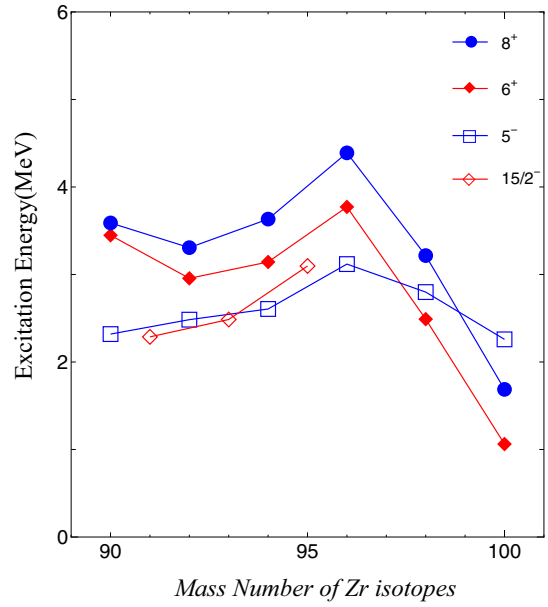

FIG. 8. Systematics of the lowest negative-parity excitations for the Zr isotopes. The 6^+ and 8^+ yrast states also are shown for comparison.

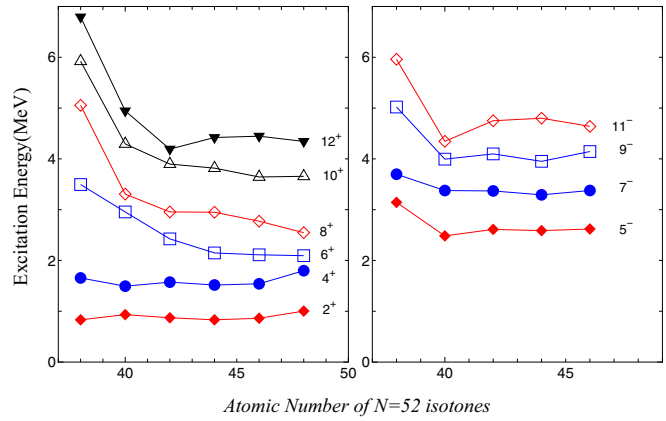

FIG. 9. Systematics of the yrast positive- and negative-parity states for the $N = 52$ even-A isotones.

comparison. It can be seen that the upward trend continues until the $N = 56$ subshell closure is reached. These features can be interpreted in terms of the tensor force. As described by Otsuka *et al.* [24], one can have a robust picture of the proton-neutron interaction in which $j_<$ and $j'_>$ orbits (or vice versa) attract each other, but the $j_>$ and $j'_>$ (or $j_<$ and $j'_<$) orbits repel each other. Here, we assume that the protons are in either $j_> = l + 1/2$ or $j_< = l - 1/2$ orbits, whereas the neutrons are in either $j'_> = l' + 1/2$ or $j'_< = l' - 1/2$ orbits with orbital angular momenta being denoted by l or l'. In this case in particular, the interaction between $\pi 2p_{1/2}$ and $\nu 2d_{5/2}$ is attractive, whereas that between $\pi 1g_{9/2}$ and $\nu 2d_{5/2}$ is repulsive. Therefore, the excitation of a proton from $2p_{1/2}$ to $1g_{9/2}$ costs more energy as more neutrons are added to the $2d_{5/2}$ orbit.

The same picture can be applied to interpret the general behavior of the yrast positive- and negative-parity states through the $N = 52$ even-A isotones. Systematics of those states are shown in Fig. 9. It is noticeable that the level structure evolves gradually from a multipletlike structure to an equidistant vibrational-like structure toward the midshell point for both the positive- and the negative-parity yrast states as the $1g_{9/2}$ orbital becomes occupied by more and more protons. This is because collectivity increases toward the midshell point in the $\pi 1g_{9/2}$ shell since the energy gap between $\nu 1g_{7/2}$ and $\nu 2d_{5/2}$ decreases due to the tensor force. The multipletlike structure of the negative-parity states in ^{92}Zr revealed in this experiment fits nicely into the systematics.

IV. SUMMARY

We have investigated the nuclear structure of ^{92}Zr via the inverse reaction ^{9}Be(^{86}Kr,$3n$)^{92}Zr. Although we could not extend the level scheme to higher-spin states, seven transitions were newly observed in the intermediate-spin region, and the lifetime was extracted for the 10_1^+ state by analysis of Doppler-broadened line shapes of decay γ rays. A large $B(E2)$ value was obtained for the transition between the 10_1^+ and the 8_1^+ states, and the magnitude was comparable to that for the deformed excited configurations in ^{94}Zr that have recently been established. A possible origin for such collectivity

was discussed qualitatively based on a phenomenological deformed rotor model. Moreover, a multipletlike structure for the negative-parity yrast states was identified. This structure fits nicely into the systematics for $N = 52$ even-A isotones.

ACKNOWLEDGMENT

We thank the crew operating the JAEA tandem accelerator for providing the heavy-ion beams used in the experiment.

[1] K. Heyde and J. L. Wood, Rev. Mod. Phys. **83**, 1467 (2011).
[2] A. Holt, T. Engeland, M. Hjorth-Jensen, and E. Osnes, Phys. Rev. C **61**, 064318 (2000).
[3] W. Urban, J. L. Durell, A. G. Smith, W. R. Phillips, M. A. Jones, B. J. Varley, T. Rząca-Urban, I. Ahmad, L. R. Morss, M. Bentaleb *et al.*, Nucl. Phys. **A689**, 605 (2001).
[4] A. Chakraborty, E. E. Peters, B. P. Crider, C. Andreoiu, P. C. Bender, D. S. Cross, G. A. Demand, A. B. Garnsworthy, P. E. Garret, G. Hackman *et al.*, Phys. Rev. Lett. **110**, 022504 (2013).
[5] C. Kremer, S. Aslanidou, S. Bassauer, M. Hilcker, A. Krugmann, P. von Neumann-Cosel, T. Otsuka, N. Pietralla, V. Y. Ponomarev, N. Shimizu *et al.*, Phys. Rev. Lett. **117**, 172503 (2016).
[6] C. Fransen, V. Werner, D. Bandyopadhyay, N. Boukharouba, S. R. Lesher, M. T. McEllistrem, J. Jolie, N. Pietralla, P. von Brentano, and S. W. Yates, Phys. Rev. C **71**, 054304 (2005).
[7] D. Pantelica, I. G. Stefan, N. Nica, M. G. Porquet, G. Duchêne, A. Astier, S. Courtin, I. Deloncle, F. Hoellinger, A. Bauchet *et al.*, Phys. Rev. C **72**, 024304 (2005).
[8] K. Sieja, F. Nowacki, K. Langanke, and G. Martínez-Pinedo, Phys. Rev. C **79**, 064310 (2009).
[9] T. Togashi, Y. Tsunoda, T. Otsuka, and N. Shimizu, Phys. Rev. Lett. **117**, 172502 (2016).
[10] B. A. Brown, D. B. Fossan, P. M. S. Lesser, and A. R. Poletti, Phys. Rev. C **14**, 602 (1976).
[11] G. Korschinek, M. Fenzl, H. Hick, A. J. Kreiner, W. Kutschera, E. Nolte, and H. Morinaga, Proc. Intern. Conf. Nucl. Structure, Tokyo **1**, 326 (1977).
[12] N. Fotiades, J. A. Cizewski, J. A. Becker, L. A. Bernstein, D. P. McNabb, W. Younes, R. M. Clark, P. Fallon, I. Y. Lee, A. O. Macchiavelli *et al.*, Phys. Rev. C **65**, 044303 (2002).
[13] P. H. Regan, N. J. Thompson, A. B. Garnsworthy, H. C. Ai, L. Amon, R. B. Cakirli, R. F. Casten, C. R. Fitzpatrick, S. J. Freeman, G. Gurdal *et al.*, in *12th International Symposium on Capture Gamma-Ray Spectroscopy and Related Topics*, edited by A. Woehr and A. Aprahamian, AIP Conf. Proc. No. 819 (AIP, New York, 2006), p. 35.
[14] Z. G. Wang, M. L. Liu, Y. H. Zhang, X. H. Zhou, S. Guo, J. G. Wang, X. G. Lei, Y. Zheng, Y. D. Fang, Y. H. Qiang *et al.*, Phys. Rev. C **89**, 044308 (2014).
[15] H. Mach, E. K. Warburton, W. Krips, R. L. Gill, and M. Moszyński, Phys. Rev. C **42**, 568 (1990).
[16] D. Bucurescu, I. Căta-Danil, G. Ciocan, C. Costache, D. Deleanu, R. Dima, D. Filipescu, N. Florea, D. G. Ghiţă, T. Glodariu *et al.*, Nucl. Instrum. Methods Phys. Res., Sect. A **837**, 1 (2016).
[17] K. Furuno, M. Oshima, T. Komatsubara, K. Furutaka, T. Hayakawa, M. Kidera, Y. Hatsukawa, M. Matsuda, S. Mitarai, T. Shizuma *et al.*, Nucl. Instrum. Methods Phys. Res., Sect. A **421**, 211 (1999).
[18] M. Oshima, Y. Toh, Y. Hatsukawa, M. Koizumi, A. Kimura, A. Haraga, M. Ebihara, and K. Sushida, J. Radiol. Nucl. Chem. **278**, 257 (2008).
[19] D. C. Radford, Nucl. Instrum. Methods Phys. Res., Sect. A **361**, 297 (1995).
[20] M. Piiparinen, A. Ataç, J. Blomqvist, G. B. Hagemann, B. Herskind, R. Julin, S. Juutinen, A. Lampinen, J. Nyberg, G. Sletten *et al.*, Nucl. Phys. **A605**, 191 (1996).
[21] J. C. Wells and N. R. Johnson, Oak Ridge National Laboratory Report No. ORNL-6689, 1991 (unpublished).
[22] L. C. Northcliffe and R. F. Schilling, At. Data Nucl. Data Tables **7**, 233 (1970).
[23] F. James and M. Roos, Comput. Phys. Commun. **10**, 343 (1975).
[24] T. Otsuka, T. Suzuki, R. Fujimoto, H. Grawe, and Y. Akaishi, Phys. Rev. Lett. **95**, 232502 (2005).